Journal of Systems Engineering and Electronics
Vol. PP, No. 99, September 2024, pp.1 – 13

Low-frequency signal generation in space based on high-frequency electric-antenna array and Doppler effect

CUI Anjing[1,2], LI Daojing[1,*], WU Jiang[1,2], GAO Jinghan[1,2], ZHOU Kai[1,2], HU Chufeng[3], WU Shumei[1], SHI Danni[4], and LI Guang[4]

1. National Key Laboratory of Microwave Imaging, Aerospace Information Research Institute, Chinese Academy of Sciences, Beijing 100190, China; 2. School of Electronic, Electrical and Communication Engineering, University of Chinese Academy of Sciences, Beijing 100049, China; 3. National Key Laboratory of Science and Technology on Unmanned Aerial Vehicle, Northwestern Polytechnical University, Xi'an 710065, China; 4. Beijing BBEF Science & Technology Co., Ltd., Beijing 100020, China

Abstract: Low-frequency signals have been proven valuable in the fields of target detection and geological exploration. Nevertheless, the practical implementation of these signals is hindered by large antenna diameters, limiting their potential applications. Therefore, it is imperative to study the creation of low-frequency signals using antennas with suitable dimensions. In contrast to conventional mechanical antenna techniques, our study generates low-frequency signals in the spatial domain utilizing the principle of the Doppler effect. We also defines the antenna array architecture, the timing sequency, and the radiating element signal waveform, and provides experimental prototypes including 8/64 antennas based on earlier research. In the conducted experiments, 121 MHz, 40 MHz, and 10 kHz composite signals are generated by 156 MHz radiating element signals. The composite signal spectrum matches the simulations, proving our low-frequency signal generating method works. This holds significant implications for research on generating low-frequency signals with small-sized antennas.

Keywords: frequency conversion, array signal processing, experimental verification, Doppler effect.

DOI: 10.23919/JSEE.2024.000079

1. Introduction

In order to achieve efficient emission of electromagnetic waves, it is necessary for the conventional electric antenna to have a size that corresponds to one-fourth of the wavelength of the signal. This limitation poses challenges for the utilization of low-frequency (LF) and very-LF (VLF) electromagnetic waves. The investigation of the technology for generating LF/VLF signals using high-frequency (HF) antennas with suitable dimensions holds significant value in the domains of target identification [1,2] and geological exploration [3,4].

Currently, large-scale land-based systems [5,6] are typically used to emit LF/VLF signals. However, this solution presents challenges including large sizes, stringent requirements for geological structures and geographical environments, as well as high power supply capacity. These complexities make it difficult to implement on mobile platforms. Research has been conducted on mechanical antennas [7−12] that utilize the principle of magnetoelectric interaction in order to reduce their dimensions. However, owing to antenna volume, driving structure, materials and other factors, the frequency flexibility and radiation intensity of the solution, as well as the operating distance are limited [13−18].

Our method employs the electric antenna array and introduces an innovative technique for generating LF/VLF signals in space. The method for generating LF signals using an electric antenna array was introduced in [19]. This method facilitates the simultaneous generation of signals with diverse frequencies in multiple orientation, hence allowing for the target detection through the utilization of a multiband antenna array [20].

In a following study, an investigation which integrated the special array structure and radiating element (RE) signal waveform was conducted in [21], and a novel approach for creating VLF signals was put forth. In con-

Manuscript received April 09, 2023.
*Corresponding author.
This work was supported by the Science and Technology Project of Aerospace Information Research Institute, Chinese Academy of Sciences (Y910340Z2F) and the Science and Technology Project of BBEF (E3E2010201).

junction with the transient electromagnetic scattering technique [22], this methodology presents an innovative approach to geological investigation through the utilization of mobile platforms.

The method in [19] and [21] possesses the following characteristics:

(i) Fundamentals of frequency conversion: based on the principles of the Doppler effect [23], emitted by the leaving radar and detected in the stationary target region, the frequency of the signal lowers.

(ii) Description in physics: the array structure emulates the signal generated when the radar leaves at a velocity close to that of light. The utilization of the array structure and RE signals makes it possible to simulate the rapid motion of radar, while also constructing the LF/VLF signal within the spatial domain.

(iii) Enhancement of the functionality: the spacing between the REs is decreased by staggered arrangement of arrays, which lessen the effect of harmonics. The signal of each RE is designed as a pulse signal with special initial phase of each pulse, and the rest period can be filled by broadened pulses, helping to generate the LF/VLF signal. The bandwidth and duty cycle of the RE signal are increased to enhance the energy utilization.

(iv) Explanation of the non-linear and broadband system: the generation of LF/VLF signals involves non-linear and wideband processes, which are influenced by frequency and pulse-width conversion.

We conducted the examination of the method using theoretical analysis and computer simulations. However, in order to establish the credibility and reliability, it is necessary to validate the method through physical experiments. This study is built upon the previous research conducted in [21]. We propose the utilization of a staggered array structure and periodic pulse-train signal to generate signals at frequencies of 121.35 MHz, 40 MHz, and 10 kHz, using 156 MHz RE signals. Experimental prototypes and schemes are designed for this purpose. Additionally, we introduce the implementation two experiments, which include 8 antennas and 64 antennas respectively. The results confirm the practical viability and have the potential to advance the progress of generating low-frequency signals by antennas with small size. The subsequent sections of this paper are structured in the following manner. Section 2 provides a comprehensive overview of our prior research conducted in this field. Section 3 and Section 4 introduce experiments based on 8-channel and 64-channel digital analogue converters (DACs). Section 5 outlines problems of current experiments and plans for further research.

2. Principle, method, and previous work

The Doppler effect states that when the radar moves away from the stationary receiving antenna, the frequency of the receiving signal decreases and the pulse broadens. Equations (1)−(3) show the frequency, Doppler frequency, and pulse width of the received signal, respectively.

$$f_r = \sqrt{\frac{(c-v)}{(c+v)}} f_0 , \tag{1}$$

$$f_d = f_r - f_0 = \left[\sqrt{\frac{(c-v)}{(c+v)}} - 1 \right] f_0 , \tag{2}$$

$$\tau_r = \sqrt{\frac{(c+v)}{(c-v)}} \tau_0 , \tag{3}$$

where f_0 and τ_0 are the frequency and pulse width of the radar signal, v and c are velocities of the radar and light.

It has been ensured in [19] that the composite signal of the antenna array emulates the received signal as the radar departs, by adjusting waveform, phase and time series of RE signals. Fig. 1(a) shows the discrete process of moving and emitting radar signals. The initial distance between the receiving antenna and the radar is R_0, which moves away from the receiving antenna at a speed of v, and the process is decomposed by the time interval Δt. Fig. 1(b) introduces the equivalent antenna array. The RE spacing is $v\Delta t$, REs from the near end to the far end of the array transmit signals at time interval Δt sequentially, and the initial phases of the RE signals are set specifically. When the time interval Δt is shorter than the carrier period of the RE signal, the composite signal in space is modulated multiple times in the carrier period; thus, an LF signal is generated.

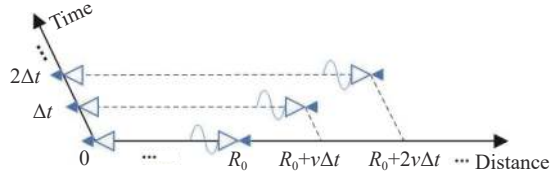

(a) Schematic diagram of decomposed process of radar motion

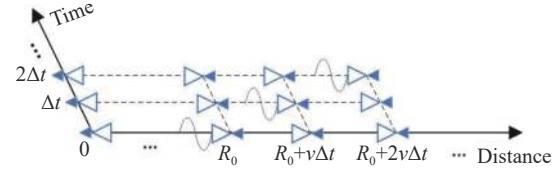

(b) Schematic diagram of equivalent radar motion generated by antenna array

Fig. 1 Equivalent radar motion based on antenna array

Based on [19], a staggered array and a periodic pulse-train signal were proposed in [21].

The structure of the staggered array is shown in Fig. 2, where λ_0 is the carrier wavelength of the RE signal, and d is RE spacing. Compared to the traditional antenna array, which limits the RE spacing to half the wavelength of the carrier, the staggered array reduces the RE spacing by arranging multiple arrays. When the REs are sufficiently small, multiple arrays form a line antenna array. By reducing the RE spacing, the staggered array reduces the time interval and improves the performance of the composite signal.

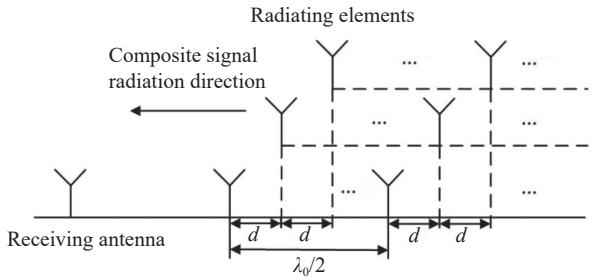

Fig. 2 Schematic diagram of staggered array structure

The waveform of the periodic pulse-train signal with a 50% duty cycle is presented in Fig. 3, where T_0 and T are the period and broadcast period of the signal. The bandwidth of the signal is determined by the pulse width, and the initial phase of each pulse is set according to the Doppler effect. Multiple periods are included in T_0, and the signals in the different broadcast periods T are the same. The RE signal is the periodic pulse-train signal, and the resting period of the signal can be filled by the broadened pulse generated by the array. Furthermore, the pulse width of the composite signal can be increased by increasing the number of periods of the signal, which is foundational for the generation of VLF signals.

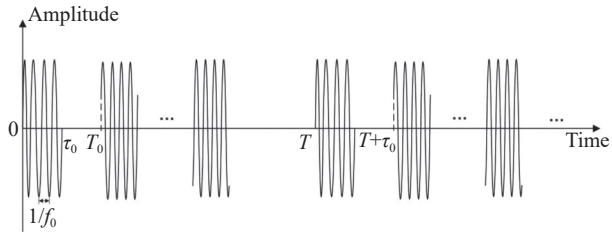

Fig. 3 Schematic diagram of RE signal

In previous work of this paper, we analyzed and derived the principle and method of LF and VLF signal generation under conditions of the antenna array and the staggered array respectively, and completed corresponding simulations with simulation software.

When the receiving antenna deviated from the direction along the array by 45°, a 400 MHz LF composite signal based on a 105 m antenna array and 1 GHz RE signals was simulated in [19], and a 10 kHz VLF composite signal generated by a 120 m staggered array and 100 MHz RE signals was simulated in [21]. Parameters such as the peak sidelobe ratio (PSLR), integral sidelobe ratio (ISLR) [24] and effective power utilization rate (EPUR) are applied to evaluate the performance of the composite signal, where the EPUR is defined as the ratio of the main lobe power of the LF signal to the power of the emission signals at the receiving antenna.

The simulation parameters in [19] and [21] are listed in Table 1, and simulation results are shown in Fig. 4. It is necessary to explain that the emission signal in the figure is the product of one RE signal and the number of REs. Because of the same spectrum of RE signals, the emission signal spectrum indicates the energy distribution of all RE signals in each frequency component. A random-phase composite signal can be generated by using RE signals with random phases, and its comparison with the composite signal illustrates the necessity of the RE signal phase setting.

Table 1 Simulation parameters of previous work

Simulation parameter	LF signal	VLF signal
Length of the array/m	105	120
Number of arrays	1	9
Equivalent spacing of RE/m	0.15	0.167
Distance/km	30	30
Number of REs	700	729
Carrier frequency of RE signal/GHz	1	0.1
Pulse width of RE signal/μs	0.73	0.115
Number of RE signal cycles	1	600
Duty cycle of RE signal/%	/	50
Phase-modulation frequency of RE signal/MHz	39	/
Phase stepping of RE signal	−10/ 13π	/
Frequency of composite signal/MHz	400	0.01
Pulse width of composite signal/μs	1.46	138.59
Sampling frequency/GHz	2	0.5
PSLR/dB	−4.28	−13.34
ISLR/dB	−14.93	−8.77
Energy ratio of LF/VLF signal in composite signal/%	96.88	88.29
EPUR/%	19.02	14.01

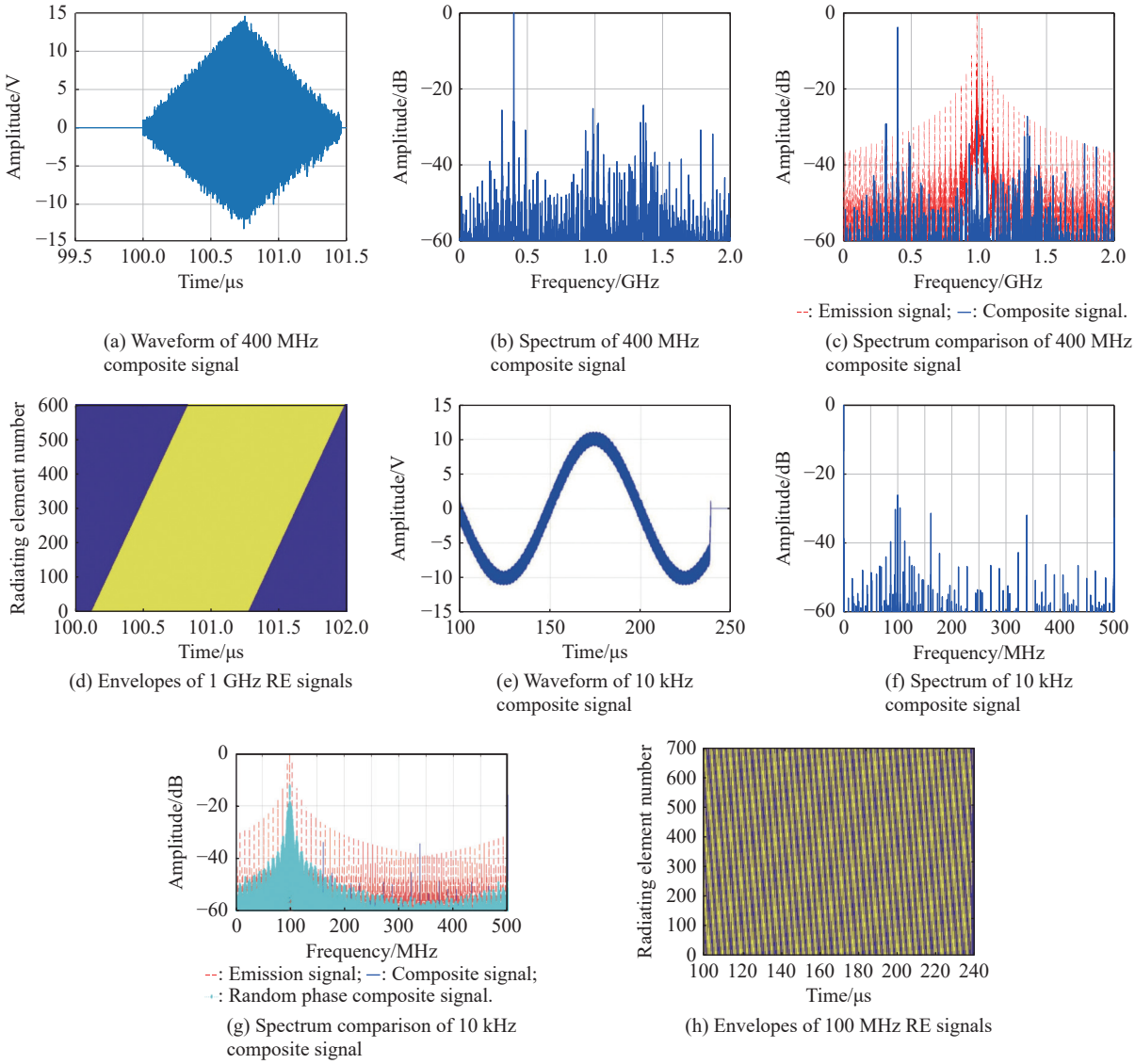

Fig. 4 400 MHz LF signal simulation based on array structure and 10 kHz VLF signal simulation based on staggered array

3. Experiment based on an 8-channel DAC

Previous studies indicate that a longer antenna array and a dense arrangement of REs enhance the performance of composite signals. However, this also requires a signal-generation system with numerous channels, which leads to a complex experimental prototype.

Under limited experimental conditions, this study aims to reduce the frequency reduction range of the composite signal and verify the effectiveness of the LF signal generation method by comparing the experimental and simulation results.

3.1 System and equipment parameters

The experimental scheme is divided into two parts, including an 8-element short-array experiment and a 64-element long-array experiment.

The REs are fed by an 8-channel digital module in the 8-element short-array experiment. As shown in Fig. 5(a), 1×8 power splitters, cables and an 8-channel digital module are combined to feed the REs in the 64-element long-array experiment, which refers to the staggered array structure shown in Fig. 2.

The RE signals are generated by a digital module, based on an 8-channel DAC. The clock frequency of the 14-bit DAC is 1 GHz, signal generation is controlled by the server, the waveform is determined by the data stored in the random access memory (RAM), and the channels of the digital module operated independently and circularly. Photographs of the digital module, server, and the waveform of the signal output are shown in Fig. 5(b) and Fig. 5(c).

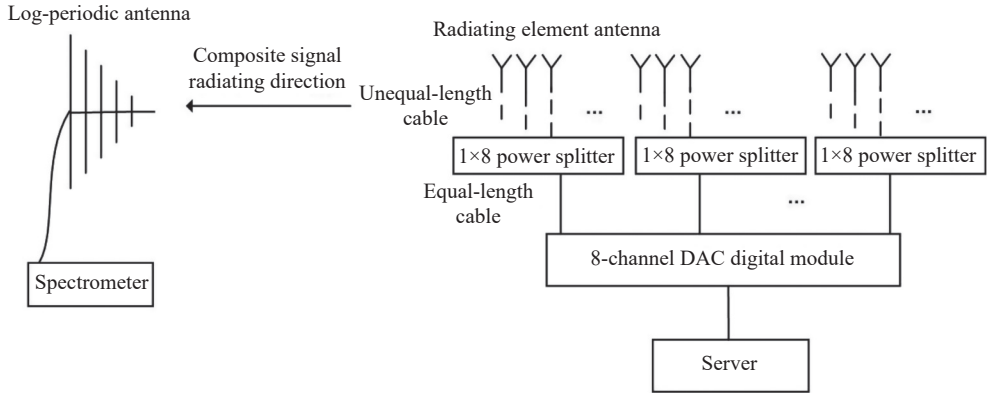

(a) Block diagram of 64-element long-array experiment

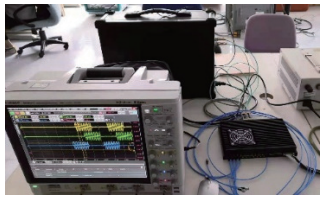

(b) Photograph of the digital module and the server

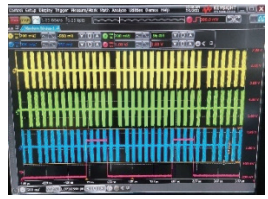

(c) Photograph of the waveform of the signal output

Fig. 5 Block diagram of 64-element long-array experiment based on 8-channel DAC and photographs of equipment and waveform of RE signals

Whip antennas (TX170) are selected as the REs. In an 8-element short-array experiment, the REs are connected to the digital module using cables. They are connected to the digital module using 1×8 power splitters and cables in a 64-element long-array experiment, and the cable lengths between the REs and power splitters vary. A log-periodic antenna is set to receive the composite signal in the direction along the array, and the signal is analyzed using a spectrometer. The parameters of the experimental equipment and the short/long-array experiment based on the 8-channel digital module are listed in Table 2, where the equivalent radar speed and frequency of the composite signal are determined by the parameters of the unequal-length cables.

Table 2 Parameters of experimental equipment

Parameter	Value
Frequency range of REs/MHz	148−175
Maximum gain of REs/dBi	3
Power capacity of REs/W	10
Input impedance of REs/Ω	50
RE direction of polarization	Vertical polarization
Radiation direction of REs	Omnidirectional
Standing-wave ratio of REs	Superior to 2 (156 MHz)
Center frequency of REs/MHz	156
Wavelength of the RE signal/m	1.923
Spacing of REs/m	0.24
Attenuation of cables/(dB·m^{-1})	<0.3
Shielding effectiveness of cables/dB	>60
Frequency range of cables/ MHz	100−18 000
Medium of cables	Poly tetra fluoro ethylene
Relative dielectric constant of cables	2.04
Isolation of power splitters/dB	>18
Standing-wave ratio of power splitters	<1.5
Frequency range of power splitters/MHz	5−1 000
Carrier frequency of RE signal/MHz	156
Carrier wavelength of RE signal/m	1.92
Spacing of RE signal/m	0.24
Pulse width of RE signal/μs	0.074
Number of RE signal pulse	13
Repetition period of digital module/μs	3
Carrier period of RE signal/ns	6.41
Ratio of equivalent radar speed and speed of light	0.246
Length of array (short/ long array)/m	1.68/ 15.12
Period of RE signal/μs	0.148
Sample frequency of digital module/GHz	1
Frequency of composite signal/ GHz	121.35

3.2 Design and test of unequal-length cables

REs in the antenna array emit periodic pulse-train signals, and formulae of the signals are illustrated in [21]. The delay and phase difference of the signals emitted by adjacent REs are as follows:

$$\Delta t = \frac{d}{v}, \tag{4}$$

$$\Delta\varphi = \varphi_{n+1} - \varphi_n = 2\pi f_0 \sqrt{1-\left(\frac{v}{c}\right)^2}\frac{d}{v}, \tag{5}$$

where N is the number of REs, and $n = 0, 1, \cdots, N-1$ is the RE serial number.

The REs are divided into multiple groups (8 REs form a group) to simplify the experimental prototype and simultaneously feed 64 REs with an 8-channel digital module at the same time. Because each channel of the digital module generates one RE signal whose phase and delay are certain, unequal-length cables are applied to generate delays and phase shifts for other RE signals in the group [25−27].

Assuming that the length difference between unequal-length cables connected to adjacent REs is l_0, the generated delay and phase shift are

$$T_D = \frac{l_0\sqrt{\varepsilon_r}}{\mathrm{c}}, \tag{6}$$

$$\Delta\varphi = \beta l_0, \tag{7}$$

where ε_r is the relative dielectric constant of the medium and β is the phase constant of the cable. By comparing (4)−(7), l_0, which determines the delay and phase change in the RE signal, can be calculated.

Through calculations and simulations, within the constraints of the experimental conditions, it is found that the composite signal performs well when l_0=0.683 m, the equivalent radar velocity is 0.246c, and the frequency of the composite signal is 121.35 MHz.

For the convenience of connecting power splitters and REs, the shortest length of unequal-length cable is set to 0.20 m, and the parameters of unequal-length cables are shown in Table 3.

Table 3 Parameters of unequal-length cables

Cable number	Length/m	Attenuation/dB	Relative phase/rad	Delay/ns
1	0.20	0.073 5	0	0.952 38
2	0.88	0.323 2	−3.109 3	4.190 5
3	1.57	0.576 7	0.111 3	7.476 2
4	2.25	0.826 4	−2.998 0	10.714
5	2.94	1.079 9	0.222 6	14.000
6	3.62	1.329 6	−2.886 7	17.238
7	4.30	1.579 4	0.287 2	20.476
8	4.99	1.832 8	−2.775 4	23.762

Power splitters and the digital module are connected to 8 m cables, and REs are connected to power splitters with unequal-lengths cables. With the experimental set-up in the spatial, time, and frequency domains, the time and phase accuracies of RE signals significantly influence the experimental results.

To test the transmission delay of the cables and power splitters, two channels of the digital module are set to emit signals, with channel 1 and channel 2 connected to the oscilloscope and the device to be tested separately. The results are displayed in Table 4; the 8 m cable (equal-length cable) and unequal-length cables are connected by a power splitter, as shown in Fig. 5(a). According to the test results, the average delay difference between the unequal-length cables is 3.258 ns. Compared with the 3.252 ns ideal delay difference, the average delay error is less than 0.01 ns (corresponding to a 2.1 mm cable length error), the mean square error is less than 0.022 ns^2, and the variation range of the delay error is within ± 0.3 ns. Thus, the transmission delay errors of the cables and power splitters slightly influence the composite signal.

Table 4 Transmission delay performance test

Device tested (Channel 0)	Delay relative to channel 1/ns	Transmission delay/ns	Delay difference/ns
Without cable	13.333	0	−
8 m cable	24.778	11.445	−
8 m cable and 0.20 m cable	27.079	13.746	−
8 m cable and 0.88 m cable	30.225	16.892	3.146
8 m cable and 1.57 m cable	33.371	20.038	3.146
8 m cable and 2.25 m cable	36.742	23.409	3.371
8 m cable and 2.94 m cable	40.000	26.667	3.258
8 m cable and 3.62 m cable	43.371	30.038	3.371
8 m cable and 4.30 m cable	46.405	33.072	3.034
8 m cable and 4.99 m cable	49.888	36.555	3.483

3.3 Simulation and analysis

According to the experimental parameters in Table 2 and Table 3, the spectra of the 121.35 MHz composite signals based on the 8-element short array and 64-element long array in the direction along the array are simulated.

3.3.1 Simulation and analysis in an ideal scenario

The simulated composite signal spectra based on the 8-element short array and 64-element long array in the ideal case are shown in Fig. 6(a) and Fig. 6(c). Spectrum comparisons of the emission, composite, and random-phase composite signals are presented in Fig. 6(b) and Fig. 6(d), and the comparisons indicate that the phase and delay of the RE signals are significant in the LF signal generation process.

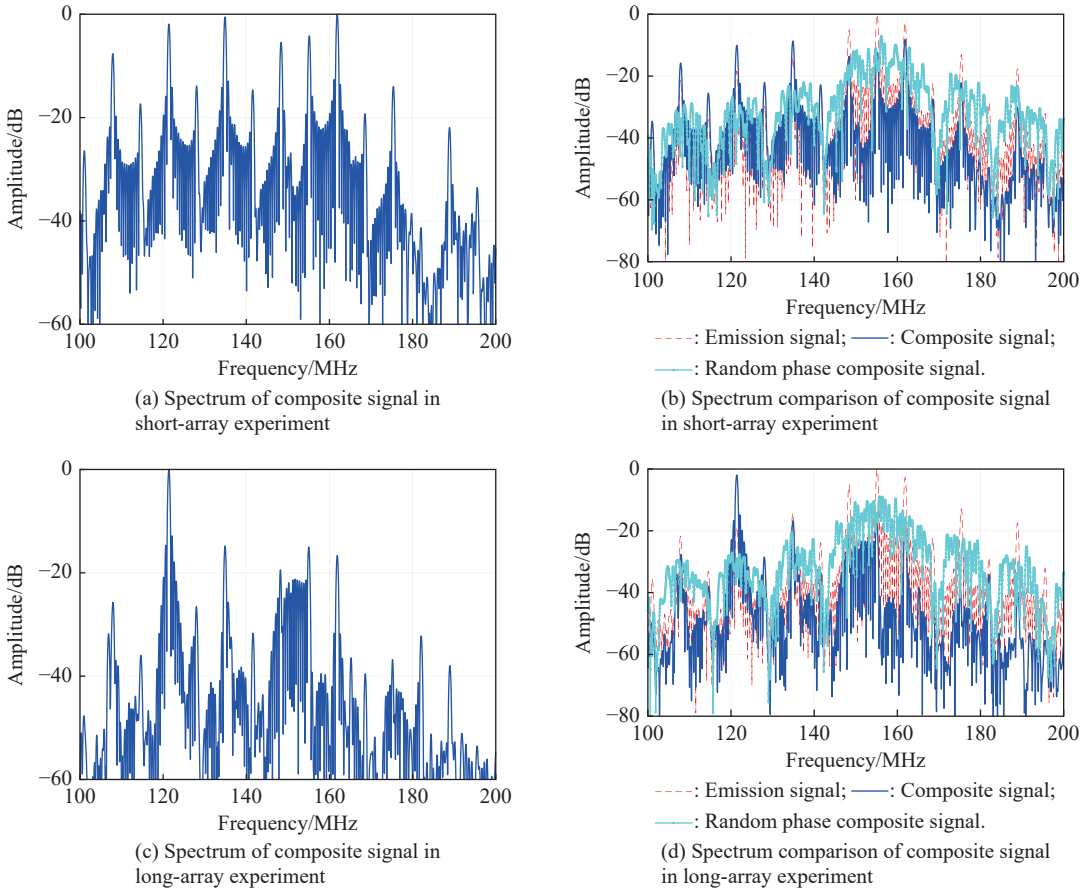

(a) Spectrum of composite signal in short-array experiment

(b) Spectrum comparison of composite signal in short-array experiment

(c) Spectrum of composite signal in long-array experiment

(d) Spectrum comparison of composite signal in long-array experiment

Fig. 6 Spectrum simulation of short/long-array experiment

In the experiment involving a short array, fewer REs and closer proximity distance between the receiving antenna and the array led to an increase in the carrier and harmonic components. Simulation results demonstrate that the composite signal based on the short array can generate a significant low-frequency component. Meanwhile, PSLR of the composite signal based on the long array is −14.818 2 dB, ISLR is −6.947 9 dB (83.20%), and EPUR is approximately 28.87%.

3.3.2 Simulation and analysis of error influence

Random and system errors exist in short/long-array experiments. Simulation and analysis indicate that ±0.5 cm spacing error, ±1 ns delay error and ±10° phase error of RE signals, and ±0.05 normalization amplitude error (corresponding to −0.45 dB to 0.42 dB) slightly affect the composite signal when the errors above are random and distributed uniformly. During the experiment, the parameter errors of the prototype are controlled within the above ranges. Therefore, the influence of system errors is simulated and analyzed in this subsection.

The clock frequency and time resolution of the digital module are 1 GHz and 1 ns, respectively. And delay system error may occur, which is less than 1 ns and exists in the short/long-array experiment. In long-array experiments, the power splitters and REs are connected by cables, which could lead to phase system errors [28,29]. Owing to the limitations of the experimental environment and the power of the RE signals, the receiving antenna is close to the antenna array, which causes the amplitudes of the received RE signals to differ, and affects the performance of the composite signal.

The simulated composite signal spectra based on the short and long array under the influence of the system errors are shown in Fig. 7(a) and Fig. 7(b), respectively. Fig. 7(a) presents the composite signal spectrum based on the short array when the receiving antenna is 6 m away from the array and a 0.1 ns delay system error exists. Fig. 7(b) shows the composite signal spectrum based on the long array when the receiving antenna is 20 m away from the array with a 0.1 ns delay system error and 30° phase system error. After accumulation, the delay system error can reach 0.7 ns. When system errors exist, the simulation results indicate that the delay system error slightly affects the composite signal of the short array, whereas the simultaneous delay error and phase system error lead to an increase in the carrier component of the composite signal based on the long array.

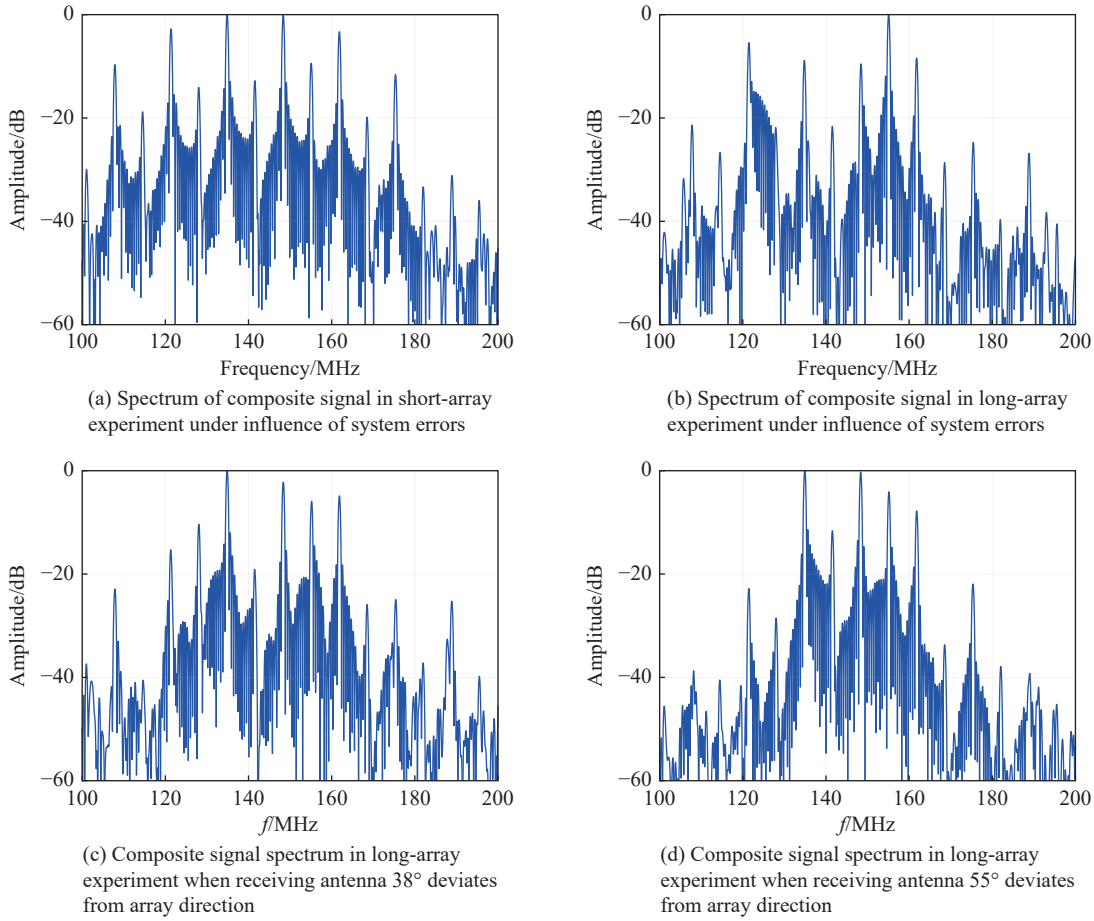

(a) Spectrum of composite signal in short-array experiment under influence of system errors

(b) Spectrum of composite signal in long-array experiment under influence of system errors

(c) Composite signal spectrum in long-array experiment when receiving antenna 38° deviates from array direction

(d) Composite signal spectrum in long-array experiment when receiving antenna 55° deviates from array direction

Fig. 7 System error analysis of short/long-array experiment

The phase of the RE signal is designed based on the parameters when the receiving antenna is set along the array. When the receiving antenna deviates from the direction along the array, the composite signal frequency is higher than the designed frequency. When the receiving antenna is located in the normal direction of array, the peak frequency of the composite signal is similar to that of the RE signals. When the receiving antenna is 22 m/24 m away from the array's near end, deviating 38°/55° from the array direction, the simulated composite signal spectra are displayed in Fig. 7(c) and Fig. 7(d), and they are influenced by the system errors in Fig. 7(b). The peak frequencies of those composite signals are 134.892 MHz and 134.907 MHz.

3.4 Experiments and analysis

3.4.1 8-element short-array experiment

The 8-element short-array experiment is completed in the anechoic chamber of Northwestern Polytechnical University and the rooftop of Aerospace Information Research Institute. Considering the influence of the experimental background, the anechoic chamber can provide an ideal experimental environment. However, the outdoor experiment provides the desired outcomes if no interfering frequency exists near the composite signal frequency. Fig. 8(a) and Fig. 8(b) show photographs of the experiment.

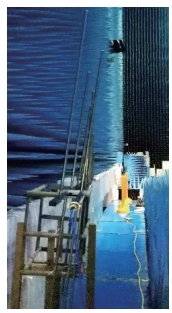

(a) Photograph of experiment in anechoic chamber

(b) Photograph of experiment on rooftop

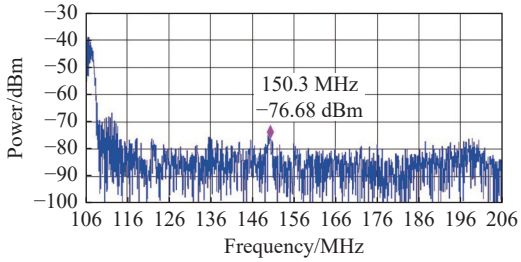

(c) Experimental background

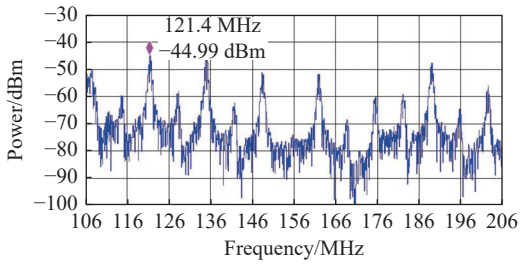

(d) Spectrum of composite signal

Fig. 8 Photographs and results of 8-channel-DAC-based short-array experiments

With the experimental background shown in Fig. 8(c), all REs of the short array are fed by the digital module, and the outdoor experimental result is shown in Fig. 8(d). The experiment results show that a 121.35 MHz composite signal is successfully generated, and the measured spectrum is similar to that of the simulation.

3.4.2 Equivalent verification experiment based on unequal-length cables and power splitters

On the ideal condition, 64 REs require 64 DAC channels. To simplify the prototype, 64 REs in the long-array experiment are fed by eight equivalent units, which include an 8-channel digital module, power splitters, and unequal-length cables. Each equivalent unit comprises 1 DAC channel, 8 unequal-length cables and a 1×8 power divider.

The result of the unequal-length cable test with 1 DAC channel and 8 REs is displayed in Fig. 9. By comparing Fig. 8(d) and Fig. 9(b), the feasibility of reducing the number of DAC channels with power splitters and cables is verified.

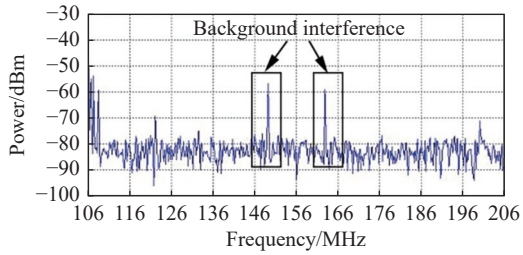

(a) Experimental background of unequal-length cable test

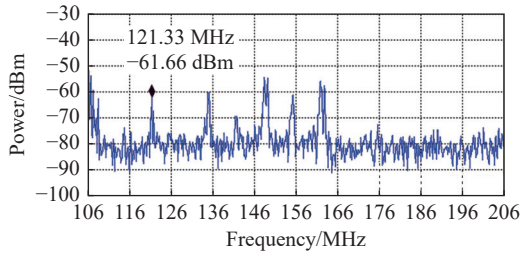

(b) Composite signal spectrum of unequal-length cable test

Fig. 9 Experiment results of the unequal-length cable test

3.4.3 64-element long-array experiment

The 64-element long-array experiments are carried out in a square, and experimental photographs are presented in Fig. 10(a) and Fig. 10(b).

(a) Photograph of receiving antenna

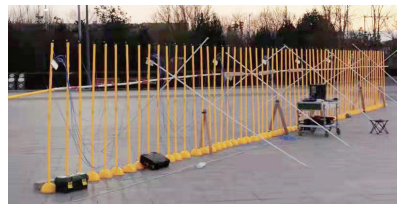

(b) Photograph of antenna array

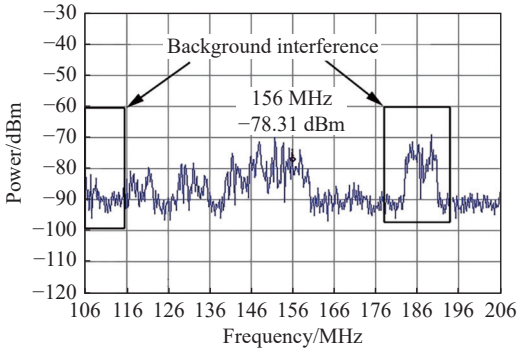

(c) Result of Experiment 1

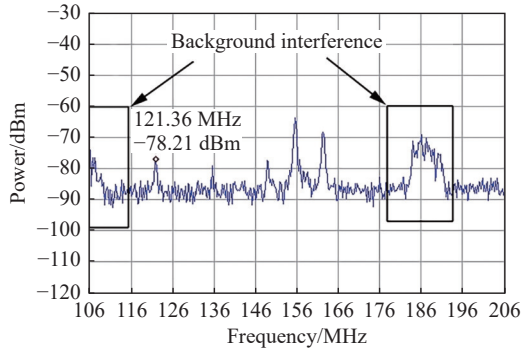

(d) Result of Experiment 2

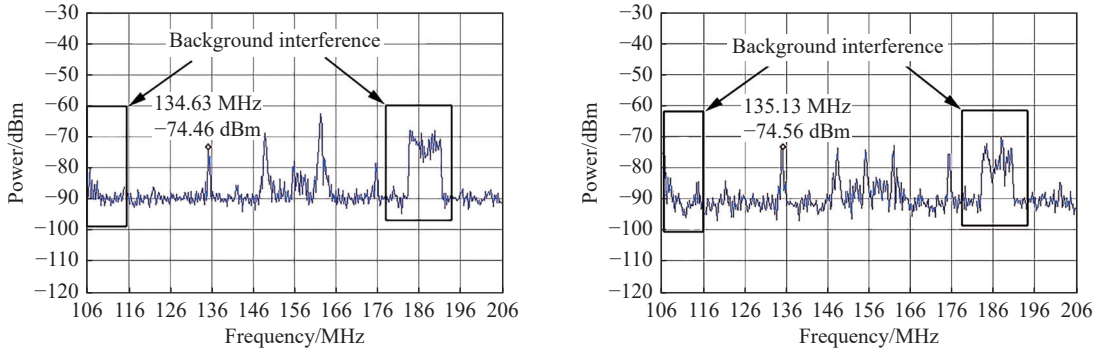

(e) Result of Experiment 3 (f) Result of Experiment 4

Fig. 10 Photographs and results of 8-channel-DAC-based long-array experiments

The composite signal spectra measured under the following experimental conditions are shown in Fig. 10(c)−Fig. 10(f):

(i) Experiment 1: RE signal with random initial phase, receiving antenna 21 m away from the near end of the array and in the array direction.

(ii) Experiment 2: RE signal with the designed initial phase, receiving antenna 21 m away from the near end of the array and in the array direction.

(iii) Experiment 3: RE signal with the designed initial phase, receiving antenna 22 m away from near end of the array, and 38° deviation from array direction.

(iv) Experiment 4: RE signal with the designed initial phase, receiving antenna 24 m away from near end of the array, and 55° deviation from array direction.

Comparing the experiment results and simulations in Fig. 10, Fig. 6 and Fig. 7, the feasibility of the LF signal generation method based on the high-frequency electric antenna array proposed in [19] and [21] is verified. The frequency and power of the composite signals variy in different directions. The receiving antenna obtain a composite signal with the lowest frequency in the array direction. When the receiving antenna deviates 90° from the array direction, the primary frequency of the composite signal matches the carrier frequency of RE signals.

4. Experiment based on a 64-channel DAC

Limited by the experimental conditions, the long-array experiment described above increases the number of digital module channels with power dividers and cables. However, the cable delay and phase shift parameters limit the frequency-reduction range of the composite signals. To further validate the proposed method, a 64-channel DAC is used to feed each RE separately, and the delay and phase of the RE signals are adjusted to generate signals with lower frequencies.

4.1 System structure and equipment parameters

A block diagram and photographs of the 64-channel-DAC-based long-array experiment are shown in Fig. 11, it can be observed that the array structure is consistent with that in Fig. 5(a). The signal of each RE is generated independently by the corresponding channel of the DAC with a sampling rate of 1.2 GSa/s, and delay and phase errors are avoided using cables of equal length. An HF handheld antenna and an LF active antenna are selected as receiving antennas. The HF handheld antenna has gains of approximately −15 dBi and −35 dBi at 156 MHz and 40 MHz, and the gain of the LF active antenna at 10 kHz frequency is approximately −78.08 dBi.

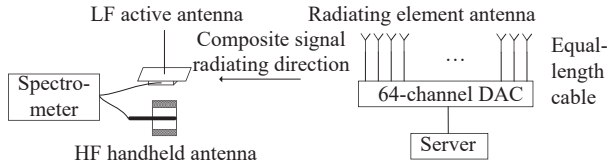

(a) Block diagram of experiment

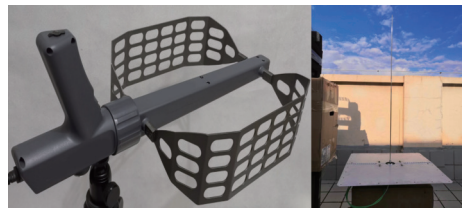

(b) Photographs of receiving antennas

(c) Photograph of 64-channel-DAC-based long array

Fig. 11 Block diagram and photographs of 64-channel-DAC-based long-array experiment

4.2 Experiments and analysis

The 64-channel-DAC-based long-array experiment is completed on the rooftop of the Aerospace Information Research Institute. The 40 MHz and 10 kHz composite signals are received by the HF handheld and LF active antennas, respectively. The simulation and experimental results are presented in Fig. 12 and Fig. 13.

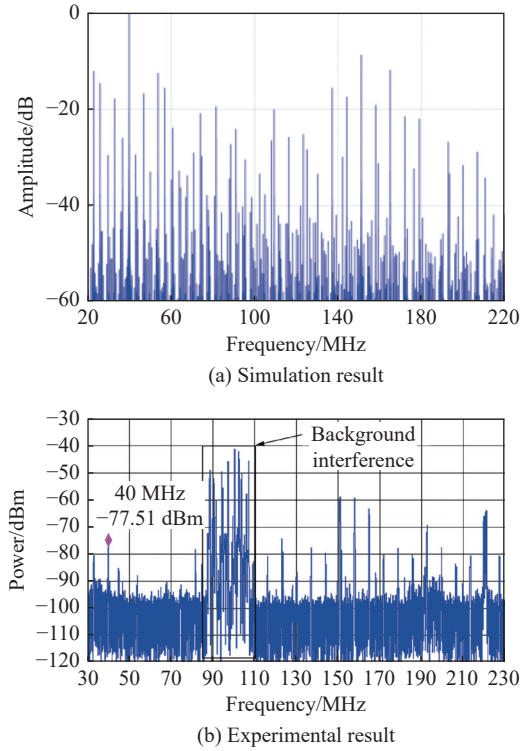

Fig. 12 Simulation and experimental result of generating a 40 MHz composite signal in 64-channel-DAC-based long-array experiment

The simulation result shown in Fig. 12(a) indicates that PSLR and EPUR of the 40 MHz LF signal composed is about 8 dB and 2.66%. Considering the 20 dB gain difference between the HF handheld antenna at 156 MHz and 40 MHz, the measured PSLR of the 40 MHz LF signal is about 6 dB, which is similar to that of the simulation. The measured result shown in Fig. 13(c) illustrates that the proposed method effectively generates a 10 kHz VLF signal using 156 MHz RE signals. The signal to noise ratio (SNR) can surpass 10 dB when the spectrometer's bandwidth is 3.6 Hz.

With the experimental validation results similar to the theoretical analysis and simulation results, it is indicated that the LF signal generation method can effectively adjust frequencies of the composite signals under the condition of the same array structure through setting RE signals, and the frequency of the LF signal composed can be lowered to the kHz level.

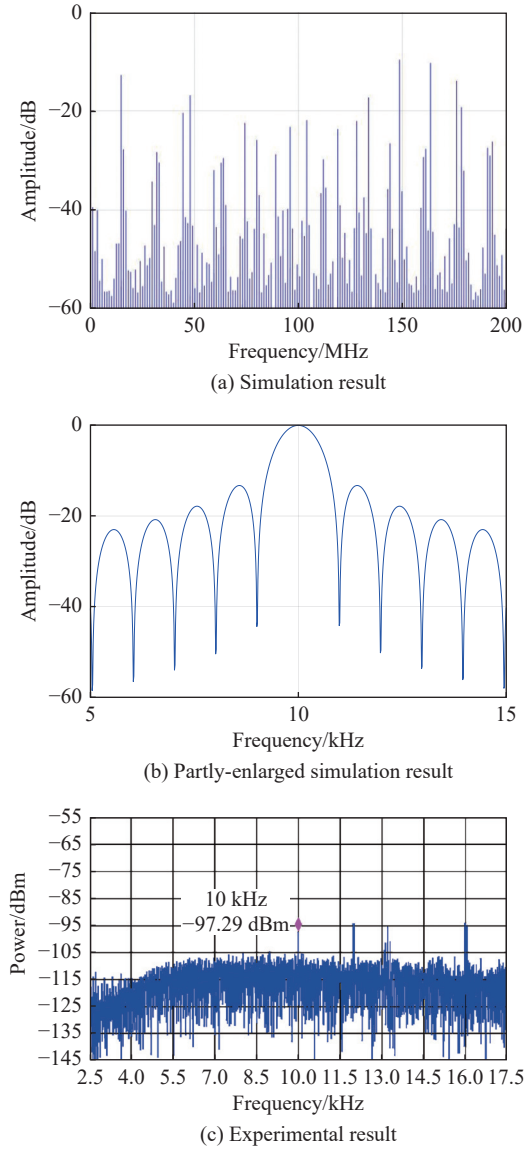

Fig. 13 Simulation and experimental result of generating a 10 kHz composite signal in 64-channel-DAC-based long-array experiment

5. Conclusions

The 8-element short-array and 64-element long-array experiments are conducted based on the 8-channel and 64-channel DACs, and 121.35 MHz, 40 MHz, and 10 kHz LF/VLF signals are generated. The frequency of the composite signal in the 8-channel-DAC-baed long-array experiment is limited by the cable parameters. To solve this issue, the prototype can introduce DACs with more channels or phase shifters [30−32] to achieve a larger range of frequency reduction. The problem of low EPUR of LF/VLF signals can be solved by increasing the array length, adding the RE number, applying REs with large bandwidth and increasing the duty cycle of RE signals. The experimental results indicate that the frequencies of

the composite signals generated by this method vary in different directions. These phenomena confirm the theoretical analysis and the proposed LF/VLF signal generation method can be applied to multiband target detection.

Omnidirectional antennas are used in simulations and experiments. Our goal is to utilize multiple REs to generate LF/VLF signals, while the array gain is not factored into consideration. In future research, the performance of the composite signal can be improved by increasing the bandwidth and duty cycle of RE signals; the beam width of the antenna array can be reduced, and the gain can be improved by constructing subarrays with REs in the pitch direction.

The LF/VLF signal generation principle in space, which combines the Doppler effect and array structure, is elucidated, and the method is preliminarily verified through physical experiments. Directional high-gain subarray structures can be adopted to form a larger effective omnidirectional radiated power. Relevant research will continue to focus on increasing the detection distance.

References

[1] KUSCHEL H, HECKENBACH J, MULLER S, et al. Countering stealth with passive, multi-static, low frequency radars. IEEE Aerospace and Electronic Systems Magazine, 2010, 25(9): 11–17.

[2] WANG X, GONG H X, ZHANG S, et al. Efficient RCS computation over a broad frequency band using subdomain MoM and Chebyshev approximation technique. IEEE Access, 2020, 8: 33522–33531.

[3] ZHOU Z M, HUANG X T. Penetration performance analysis of VHF/UHF ultra-wideband synthetic aperture radar. Systems Engineering and Electronics, 2003, 25(11): 1336–1340. (in Chinese)

[4] LU J X, ZHOU X J, LIU Y, et al. The extremely low frequency engineering project for underground exploration. Engineering, 2022, 10: 13–20.

[5] REN Y, LIN H, TIAN Y Z. A study on mechanical antenna based on rotating magnetic dipole. Modern Radar, 2020, 42(4): 68–71, 76. (in Chinese)

[6] HAO Z Y, WANG Y X, ZHOU Q, et al. System design and verification of rotating-magnet based mechanical low-frequency antenna. Journal of National University of Defense Technology, 2023, 45(1): 67–73. (in Chinese)

[7] CUI Y, WU M, SONG X, et al. Research progress of small low-frequency transmitting antenna. Acta Physica Sinica, 2020, 69(20): 171–183. (in Chinese)

[8] NAN T X, LIN H, GAO Y, et al. Acoustically actuated ultra-compact NEMS magnetoelectric antennas. Nature Communications, 2017, 8: 296.

[9] BURCH H C, GARRAUD A, MITCHELL M F, et al. Experimental generation of ELF radio signals using a rotating magnet. IEEE Trans. on Antennas and Propagation, 2018, 66(11): 6265–6272.

[10] BICKFORD J A, DUWEL A E, WEINBERG M S, et al. Performance of electrically small conventional and mechanical antennas. IEEE Trans. on Antennas and Propagation, 2019, 67(4): 2209–2223.

[11] GONG S H, LIU Y, LIU Y A. Rotating-magnet based mechanical antenna (RMBMA) for ELF-ULF wireless communication. Progress in Electromagnetics Research M, 2018, 72: 125−133.

[12] PRASAD M N S, SELVIN S, TOK R U, et al. Directly modulated spinning magnet arrays for ULF communications. Proc. of the IEEE Radio and Wireless Symposium, 2018: 171−173.

[13] FAWOLE O C, TABIB-AZAR M. An electromechanically modulated permanent magnet antenna for wireless communication in harsh electromagnetic environments. IEEE Trans. on Antennas and Propagation, 2017, 65(12): 6927–6936.

[14] M N S P, TOK R U, FEREIDOONY F, et al. Magnetic pendulum arrays for efficient ULF transmission. Scientific Reports, 2019, 9: 13220.

[15] SELVIN S, PRASAD S, HUANG Y K, et al. Spinning magnet antenna for VLF transmitting. Proc. of the IEEE International Symposium on Antennas and Propagation & USNC/URSI National Radio Science Meeting, 2017: 1477−1478.

[16] BARANI N, SARABANDI K. A frequency multiplier and phase modulation approach for mechanical antennas operating at super low frequency (SLF) band. Proc. of the IEEE International Symposium on Antennas and Propagation and USNC-URSI Radio Science Meeting, 2019: 2169−2170.

[17] REN W C, CHEN S, GAO Y, et al. Progress and technical framework of the BAW mediated magnetoelectric antenna. Chinese Journal of Radio Science, 2021, 36(4): 491–497, 510. (in Chinese)

[18] BARANI N, KASHANIANFARD M, SARABANDI K. A mechanical antenna with frequency multiplication and phase modulation capability. IEEE Trans. on Antennas and Propagation, 2021, 69(7): 3726–3739.

[19] CUI A J, LI D J, ZHOU K, et al. On method of composing low frequency signals based on array structures. Acta Physica Sinica, 2020, 69(19): 162–173. (in Chinese)

[20] RAO P H, SUJITHA S, SELVAN K T. A multiband, mutipolarization shared-aperture antenna: design and evaluation. IEEE Antennas and Propagation Magazine, 2017, 59(4): 26–37.

[21] CUI A J, LI D J, ZHOU K, et al. Research on the method of composing very low frequency signals based on the staggered array. Journal of Radars, 2020, 9(5): 925–938. (in Chinese)

[22] KUO C H, MOGHADDAM M. Electromagnetic scattering from a buried cylinder in layered media with rough interfaces. IEEE Trans. on Antennas and Propagation, 2006, 54(8): 2392–2401.

[23] WALKER J, HALLIDAY D, RESNICK R. Fundamentals of physics. Hoboken: Wiley, 2014.

[24] WEI Z Q. Synthetic aperture radar satellite. Beijing: China Science Publishing & Media Ltd, 2001. (in Chinese)

[25] SKOLNIK M. Radar handbook. McGraw-Hill: McGraw-Hill, 2008.

[26] CZUBA K, SIKORA D. Phase drift versus temperature measurements of coaxial cables. Proc. of the 18th International Conference on Microwaves, Radar and Wireless Communications, 2010.

[27] CHANG H C. Phase noise in self-injection-locked oscillators-theory and experiment. IEEE Trans. on Microwave Theory and Techniques, 2003, 51(9): 1994–1999.

[28] GE Y, HUANG H, YUAN H. Phase characteristics of coaxial cable caused by temperature and mechanical bending. Journal of Terahertz Science and Electronic Information Technology, 2019, 17(4): 621–626. (in Chinese)

[29] ZAHEDI A, ABBASI ARAND B. GA-based approach to phase compensation of large phased array antennas. Journal of Systems Engineering and Electronics, 2018, 29(4): 723–730.

[30] ZHENG S Y, CHAN W S. Differential RF phase shifter with harmonic suppression. IEEE Trans. on Industrial Electronics, 2014, 61(6): 2891–2899.
[31] LU C J, SHENG W X, HAN Y B, et al. Phase-only pattern synthesis based on gradient-descent optimization. Journal of Systems Engineering and Electronics, 2016, 27(2): 297–307.
[32] LIN Y W, CHOU Y C, CHANG C Y. A balanced digital phase shifter by a novel switching-mode topology. IEEE Trans. on Microwave Theory and Techniques, 2013, 61(6): 2361–2370.

Biographies

CUI Anjing was born in 1997. She received her B.S. degree in electronic engineering from Xidian University, Xi'an, China, in 2020. She is a doctoral student with School of Electronic, Electrical and Communication Engineering, University of Chinese Academy of Sciences, Beijing, China. Her research interest is array detector signal processing.
E-mail: cuianjing20@mails.ucas.ac.cn

LI Daojing was born in 1964. He received his B.S. and M.S. degrees from Nanjing University of Science and Technology, Nanjing, China, in 1986 and 1991, respectively. He received his Ph.D. degree from Northwestern Polytechnical University, Xi'an, China, in 2003. He is a researcher and doctoral supervisor with National Key Laboratory of Microwave Imaging, Aerospace Information Research Institute, Chinese Academy of Sciences. His research interests include radar system and radar signal processing.
E-mail: lidj@mail.ie.ac.cn

WU Jiang was born in 1999. He received his B.S. degree in communication engineering from China University of Geosciences, Wuhan, China, in 2020. He is a doctoral student with School of Electronic, Electrical and Communication Engineering, University of Chinese Academy of Sciences, Beijing, China. His interest is coherent detection infrared imaging technology.
E-mail: 15074736402@163.com

GAO Jinghan was born in 1997. He received his B.S. degree in communication engineering from Dalian Maritime University, Dalian, China, in 2020. He is a doctoral student with School of Electronic, Electrical and Communication Engineering, University of Chinese Academy of Sciences, Beijing, China. His research interests include diffractive optical system and ladar.
E-mail: gaojinghan20@mails.ucas.ac.cn

ZHOU Kai was born in 1995. He received his B.S. degree in electronic information science and technology from Central South University, Changsha, China, in 2020. He is a doctoral student with School of Electronic, Electrical and Communication Engineering, University of Chinese Academy of Sciences, Beijing, China. His research interests include infrared and laser signal multi-channel interference imaging technology.
E-mail: zk_6810@163.com

HU Chufeng was born in 1982. He received his B.S., M.S. and Ph.D. degrees in electromagnetic field and microwave technology from Northwestern Polytechnical University, Xi'an, China, in 2004, 2007 and 2010, respectively. He is a researcher with Northwestern Polytechnical University, Xi'an, China. His research interests include remote sensing, scattering measurement, and imaging techniques.
E-mail: huchufeng@nwpu.edu.cn

WU Shumei was born in 1969. She received her B.S. degree in communication engineering with School of Electronic Engineering, Beijing United University, Beijing, China. She is an associate researcher with National Key Laboratory of Microwave Imaging, Aerospace Information Research Institute, Chinese Academy of Sciences, Beijing, China. Her research interest is radar signal processing.
E-mail: wusm@aircas.ac.cn

SHI Danni was born in 1994. She received her M.S. degree in electronics and communication engineering from School of Electronic and Information Engineering, Beijing Jiaotong University, Beijing, China. She is a radio frequency engineer in Beijing BBEF Science & Technology Co., Ltd. Her research interests include electromagnetic field and electromagnetic waves.
E-mail: 837974747@qq.com

LI Guang was born in 1982. He received his B.S. degree in communication engineering from Southwest Jiaotong University, Chengdu, China, in 2005. He is a system integration engineer with Beijing BBEF Science & Technology Co., Ltd. His research interests include communications and electronic countermeasures.
E-mail: 18613819820@163.com